LETTER

Spreading continents kick–started plate tectonics

Patrice F. Rey[1], Nicolas Coltice[2,3] & Nicolas Flament[1]

Stresses acting on cold, thick and negatively buoyant oceanic lithosphere are thought to be crucial to the initiation of subduction and the operation of plate tectonics[1,2], which characterizes the present-day geodynamics of the Earth. Because the Earth's interior was hotter in the Archaean eon, the oceanic crust may have been thicker, thereby making the oceanic lithosphere more buoyant than at present[3], and whether subduction and plate tectonics occurred during this time is ambiguous, both in the geological record and in geodynamic models[4]. Here we show that because the oceanic crust was thick and buoyant[5], early continents may have produced intra-lithospheric gravitational stresses large enough to drive their gravitational spreading, to initiate subduction at their margins and to trigger episodes of subduction. Our model predicts the co-occurrence of deep to progressively shallower mafic volcanics and arc magmatism within continents in a self-consistent geodynamic framework, explaining the enigmatic multimodal volcanism and tectonic record of Archaean cratons[6]. Moreover, our model predicts a petrological stratification and tectonic structure of the sub-continental lithospheric mantle, two predictions that are consistent with xenolith[5] and seismic studies, respectively, and consistent with the existence of a mid-lithospheric seismic discontinuity[7]. The slow gravitational collapse of early continents could have kick-started transient episodes of plate tectonics until, as the Earth's interior cooled and oceanic lithosphere became heavier, plate tectonics became self-sustaining.

Present-day plate tectonics is primarily driven by the negative buoyancy of cold subducting plates. Petrological and geochemical proxies of subduction preserved in early continents point to subduction-like processes already operating before 3 billion years (Gyr) ago[8,9] and perhaps as early as 4.1 Gyr ago[10]. However, they are not unequivocal, and geodynamic modelling suggests that the thicker basaltic crust produced by partial melting of a hotter Archaean or Hadean mantle would have had increased lithospheric buoyancy and inhibited subduction[3,4]. Mantle convection under a stagnant lid with extensive volcanism could therefore have preceded the onset of subduction[11]. In this scenario, it is classically assumed that the transition from stagnant-lid regime to mobile-lid regime and the onset of plate tectonics require that convective stresses overcame the strength of the stagnant lid[12] at some stage in the Archaean.

On the modern Earth, gravitational stresses due to continental buoyancy can contribute to the initiation of subduction[2,13]. The role of continental gravitational stresses as a driver of Archaean lithospheric deformation has been emphasized[14,15]; however, their potential to initiate subduction has been overlooked. Studies of xenoliths from Archaean cratons show that the early continental crust was underlain by a thick (~200 km) lithospheric mantle, moderately to strongly depleted and therefore buoyant[5]. A common model for the formation of early continental lithosphere invokes partial melting in mantle plumes, leading to magnesium-rich mantle residues (for example, refractory harzburgites and dunites) under thick basaltic plateaux[5,16,17]. Partial melting of these thick basaltic crusts, at depths >40 km, further differentiates the crust into tonalite–trondhjemite–granodiorite (TTG) and restitic material[16,18].

First-order calculations show that the horizontal gravitational force acting between a continent 200 km thick and adjacent oceanic lithosphere is of the order of 10^{13} N m^{-1} (see Extended Data Fig. 1), comparable to that of present-day tectonic forces driving orogenesis[1]. To explore the tectonic impact of a thick and buoyant continent surrounded by a stagnant lithospheric lid, we produced a series of two-dimensional thermo-mechanical numerical models of the top 700 km of the Earth, using temperature-dependent densities and visco-plastic rheologies that depend on temperature, melt fraction and depletion, stress and strain rate (see Methods). The initial temperature field is the horizontally averaged temperature profile of a stagnant-lid convection calculation for a mantle ~200 K hotter than at present (Fig. 1A, a and Extended Data Fig. 2). The absence of lateral temperature gradients ensures that no convective stresses act on the lid, allowing us to isolate the dynamic effects of the continent. A buoyant and stiff continent 225 km thick (strongly depleted mantle root 170 km thick overlain by felsic crust 40 km thick; see Fig. 1B, a) is inserted within the lid, on the left side of the domain to exploit the symmetry of the problem (Fig. 1A, a). A mafic crust 15 km thick covers the whole system (Fig. 1A, a), consistent with the common occurrence of thick greenstone covers on continents, as well as thick basaltic crust on the oceanic lid[3].

Our numerical solutions show that the presence of a buoyant continent imparts a horizontal force large enough to induce a long period (~50–150 Myr) of slow collapse of the whole continental lithosphere (Fig. 1 and Extended Data Fig. 3), in agreement with the dynamics of spreading for gravity currents[19]. Hence, a continent of larger volume leads to larger gravitational power and faster collapse. Because of lateral spreading of the continent, the adjacent lithospheric lid is slowly pushed under its margin (Fig. 1A, b and Extended Data Fig. 3A, a). For gravitational stress lower than the yield stress of the oceanic lid, thickening of the margin of the lid is slow, and viscous drips (that is, Rayleigh–Taylor instabilities) detach from its base (Extended Data Fig. 3A, a and b). These instabilities, typical of stagnant-lid convection[20], mitigate the thermal thickening of the lid.

When gravitational stresses overcome the yield stress of the lithospheric lid, subduction is initiated (Fig. 1A, b and c). Depending on the half-width of the continent and its density contrast with the adjacent oceanic lid (that is, its gravitational power) three situations can arise: first, subduction initiates and stalls (Extended Data Fig. 3b); second, the slab detaches and the lid stabilizes (Fig. 1A, d and e and Extended Data Fig. 3c); or third, recurrent detachment of the slab continues until recycling of the oceanic lid is completed, followed by stabilization (Extended Data Fig. 3d). When the slab reaches a depth of ~200 km, slab pull contributes to drive subduction and rapid rollback of the subducting lid, which in turn promotes lithospheric boudinage and continental rifting (Fig. 1A, c and Extended Data Fig. 3C, b–d). Through spreading and thinning of the continent, its base rises from 225 km to ~75 km deep on average, and shallower between lithospheric boudins (Figs 1A, d and 2b and Extended Data Fig. 3C, c and d and D, b–f). This triggers an episode of deep (~150 km) to shallow (<100 km) decompression melting and progressive depletion of the ambient fertile mantle (Figs 2 and 3b). Harzburgites of the continental mantle are too refractory to melt on decompression. Polybaric melting of fertile mantle produces a basalt cover 6 km thick and a mantle residue ~75 km thick with an average depletion of 7.5% (Figs 2 and 3c). The bulk of depletion occurs during a volcanic episode lasting up to ~13 Myr, although partial melting persists for up to 45 Myr (Fig. 2b).

[1]Earthbyte Research Group, School of Geosciences, The University of Sydney, Sydney NSW 2006, Australia. [2]Laboratoire de Géologie de Lyon, UMR 5276 CNRS, Université Lyon 1, Ecole Normale Supérieure de Lyon, 69622 Villeurbanne Cedex, France. [3]Institut Universitaire de France, 75005 Paris, France.
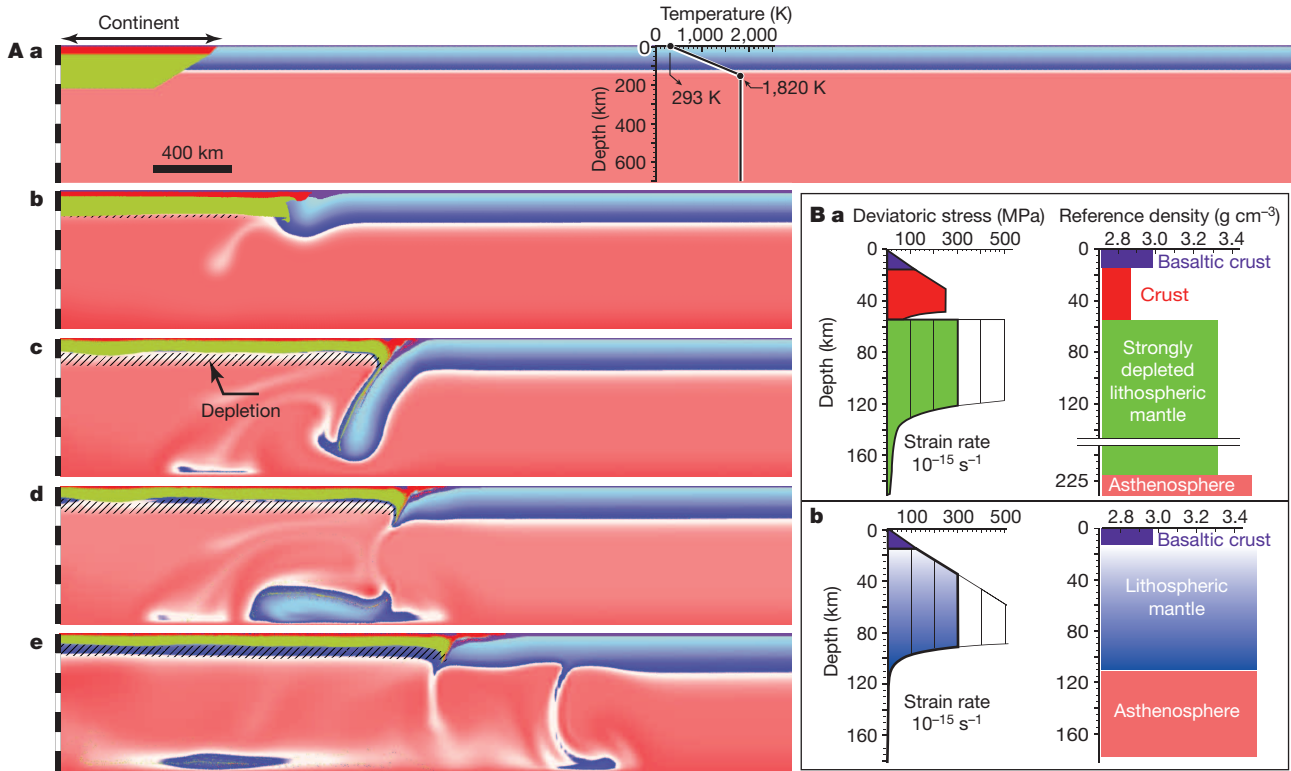
Figure 1 | Numerical solution of an example of continent collapse leading to subduction. A, a, Modelling setup (0 Myr). **b–e,** Computed snapshots for a box 700 km deep and 6,300 km long including a continent 225 km thick with a half-width of 800 km. **b,** 46.7 Myr; **c,** 55.3 Myr; **d,** 57.2 Myr; **e,** 123.8 Myr. All mantle rocks have a limiting yield stress of 300 MPa. Mantle cooler than 1,620 K is in blue (darker blue is hotter); mantle hotter than 1,620 K is in pink (darker pink is hotter). Regions of depletion due to partial melting of ambient fertile mantle are hatched. **B,** Compositional structure, reference densities and reference rheological profile for the continent (**a**) and for the adjacent lithospheric lid (**b**). This numerical solution documents the long phase of slow continental spreading leading to the initiation of a slab (**A, b** and **c**). Once the slab has reached a depth of ~200 km, slab pull contributes to drive subduction, rollback and continental boudinage (**A, c**) (in some experiments boudinage leads to rifting) and slab detachment (**A, d**). In this experiment the detachment of the slab is followed by a long period of thermal relaxation and stabilization during which the thickness of the continent increases through cooling and incorporation of the moderately depleted mantle (**A, e**).
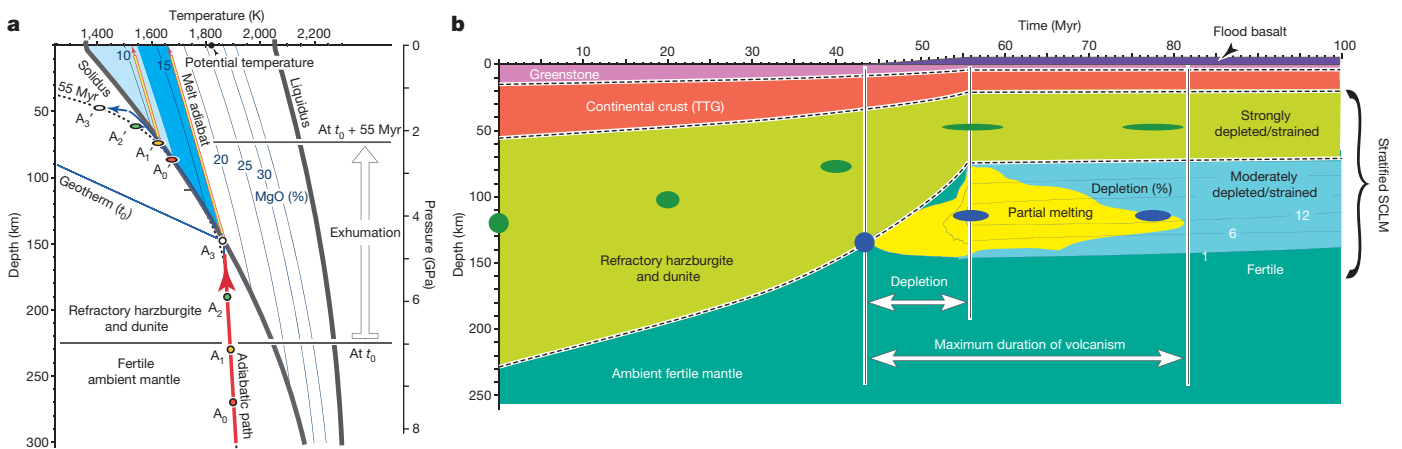
Figure 2 | Development of layering of the continental lithosphere through thinning and progressive accretion of moderately depleted mantle. a, Points located at depths A_0 to A_3 before spreading are exhumed during spreading to locations A_0' to A_3', following the blue pressure–temperature–time path. The geotherm intersects the solidus, and the temperature in the partially molten column remains close to the solidus because latent heat is continuously extracted with the melt once melt fraction has reached 1%. Melt is extracted from various depths following the melt adiabat (yellow paths). The region between the solidus and liquidus of the hydrous fertile mantle is mapped for MgO content (see Methods). The deeper part of the column produces komatiitic basalts (dark blue shading), whereas partial melting at pressures <3 GPa produces tholeiitic basalts (pale blue shading). **b,** Temporal evolution of the laterally averaged depletion (blue), partial melting (yellow) and density interfaces (thick dashed lines). As spreading and thinning proceed, pure shear fabrics (shown as finite strain ellipses) develop in the refractory mantle and in the moderately depleted mantle, which records a shorter strain history. The base of the partially molten column remains close to ~150 km, whereas its top progressively rises from ~150 km at the beginning of partial melting (at ~44 Myr) to an average of ~75 km below the surface (at ~55 Myr). From 55 Myr, spreading slows down and progressive cooling reduces the amount of melt, until partial melting stops at ~82 Myr. This results in the progressive chemical and structural stratification of the lithospheric mantle.
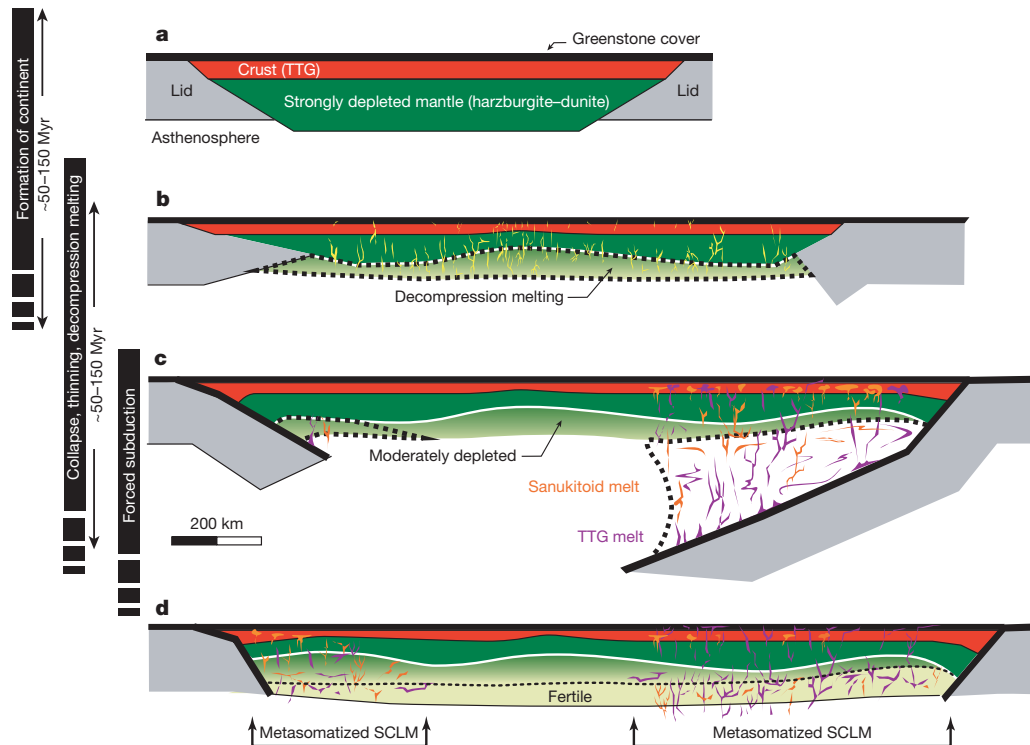
Figure 3 | Proposed model for the co-evolution of cratonic crust and sub-continental lithospheric mantle. Integration of the results of our numerical experiments with petrological data supports a model linking the formation of continents to the initiation of subduction at their margins, through the process of continent collapse. This model predicts the layering of the sub-continental lithospheric mantle (SCLM), polybaric and multimodal volcanism recorded in greenstone cover, and the metasomatism of the SCLM. **a**, Partial melting in the deep mantle leads to the formation of an oceanic plateau that differentiates into a continent. The residue of mantle melting forms the strongly depleted harzburgite root of the continent, whereas the deeper part of the basaltic crust differentiates by partial melting into TTG. **b**, As the continent grows in thickness and length, excess gravitational potential energy drives its collapse and the shortening of the adjacent oceanic lid (in grey). During collapse and thinning of the continent, decompression melting of the fertile ambient mantle and extraction of deep (komatiitic basalt) to shallow (tholeiite) melts (yellow) contribute to the growth of the greenstone cover, and to the formation of a moderately depleted mantle layer. **c**, As a result of the horizontal push of the collapsing continent, the thickened margin of the oceanic lid subducts underneath the continental margin. Partial melting of the thick, eclogitized oceanic crust produces TTG melts (purple), which metasomatise both the mantle wedge and the lithospheric mantle. Melting of the hydrated and metasomatized mantle wedge produces calc-alkaline to sanukitoid melts (orange). **d**, After detachment of the slab, and once the gravitational power of the continent is too small to deform its surrounding, the continent thickens through thermal relaxation and cooling, first incorporating the layer of moderately depleted mantle and then a layer of unmelted fertile mantle.

In the last ~25 Myr of melting, the sub-continental mantle cools until melting stops (Figs 1A, e and 2). Decompression melting allows the spreading continent to maintain a minimum chemical thickness of at least 140–150 km. After the melting phase, conductive cooling results in the thermal thickening and strengthening of a chemically stratified cratonic lithosphere (Figs 1A, e, 2 and 3d). Over the whole process, the buoyancy of the continent decreases, subduction stops and a stagnant lid regime is re-established (Fig. 1A, e).

Trade-offs between yield stress, gravitational stress and continental volume determine the initiation of subduction in our models (Extended Data Fig. 3b, d). For a yield stress of 150–300 MPa, consistent with recent estimates of rheological parameters of the lithospheric mantle[21,22], increasing the width of the continent favours the initiation of subduction (Extended Data Fig. 4). These results suggest an increasing potential for subduction as continental area increased over time.

Not only do our models confirm important results from previous studies, but they also provide innovative explanations for key attributes of Archaean cratons. Both transient subduction and dripping styles are consistent with previous models of Archaean[23] and modern[13] subduction. As observed in previous work, the length of the detached segments increases with the yield stress of the lid[23]. Our models confirm that a combination of the buoyancy and high viscosity of Archaean sub-continental lithospheric mantle, and large plastic strain weakening, prevent the re-cycling of the sub-continental lithospheric mantle, which explains its longevity[24]. Our models account for the average thickness (~6 km) and duration of volcanism (~10–50 Myr) of greenstone covers, and predict polybaric (5–2 GPa) partial melting, involving deep (garnet-bearing) to shallow sources (Fig. 2). The MgO content of basaltic melts produced at these pressures ranges between 11% and 17% (Fig. 2a), consistent with the komatiitic basalts (12–18% MgO) typical of Archaean greenstones[17,25]. In our model, tholeiitic basalts (6–12% MgO), abundant in Archean greenstones[25], can be produced in regions of continental necking where partial melting can occur at pressures <3 GPa. Figure 2a shows that to account for the formation of komatiites (MgO > 18%) our model would simply require a mantle potential temperature greater than 1,820 K. When subduction starts, arc volcanism is expected at convergent margins while continental extension and rifting still operate (Fig. 1A, c). Our model can therefore explain the metasomatism and production of sanukitoid melts through the migration of younger TTG melts generated by the partial melting of subducting eclogitized basaltic crust (Fig. 3c).

On modern Earth, mantle plumes mostly occur away from subduction zones[26]. Hence, the eruption duration and sequential interlayering of komatiite, tholeiite, calc-alkaline and felsic volcanics, ubiquitous in Archaean greenstone belts[25,27,28], frequently attributed to repeated interaction between mantle plumes and subduction zones over hundreds of millions of years[6], remains enigmatic. However, our model predicts this co-occurrence of deep (up to 150 km) to shallow (<100 km) mafic volcanics (Fig. 2b) and arc magmatism, in a self-consistent geodynamic framework.

Moreover, our model predicts a progressive chemical stratification of the sub-continental lithospheric mantle concomitant with that of the

continental crust and growth of the greenstone cover. This is consistent with the strong geochemical layering of cratonic mantle inferred by geochemical and petrological studies of mantle xenoliths[5]. Pure shear stretching and thinning during the collapse promotes development of a subhorizontal litho-tectonic fabric in the refractory harzburgite and dunite, and to a smaller extent in the accreted moderately depleted mantle (Fig. 2b). The predicted litho-tectonic layering can explain the seismic mid-lithospheric discontinuity at about 100 km depth observed within cratons[29]. This discontinuity[7] could correspond to the sharp transition predicted by our model between the strongly stretched, strongly depleted primary root of the continent and the moderately stretched, moderately depleted-to-fertile mantle accreted through cooling (Fig. 3).

We propose that the collapse of early continents was a key process in Archaean geodynamics, resulting in the concomitant structuration of the mantle root and the crust of cratons. This process would have kick-started transient episodes of plate tectonics, until plate tectonics became self-sustaining through the increasing continental area[30] and the decreasing buoyancy of oceanic plates[3].

Online Content Methods, along with any additional Extended Data display items and Source Data, are available in the online version of the paper; references unique to these sections appear only in the online paper.

1. Bott, M. H. P. Modelling the plate-driving mechanism. *J. Geol. Soc. Lond.* **150**, 941–951 (1993).
2. Faccenna, C., Giardini, D., Davy, P. & Argentieri, A. Initiation of subduction at Atlantic-type margins: insights from laboratory experiments. *J. Geophys. Res.* **104**, 2749–2766 (1999).
3. Sleep, N. H. & Windley, B. F. Archean plate tectonics: constraints and inferences. *J. Geol.* **90**, 363–379 (1982).
4. van Hunen, J. & Moyen, J. F. Archean subduction: fact or fiction? *Annu. Rev. Earth Planet. Sci.* **40**, 195–219 (2012).
5. Griffin, W. L., O'Reilly, S. Y., Afonso, J.-C. & Begg, G. C. The composition and evolution of lithospheric mantle: a re-evaluation and its tectonic implications. *J. Petrol.* **50**, 1185–1204 (2009).
6. Wyman, D. A., Kerrich, R. & Polat, A. Assembly of Archean cratonic mantle lithosphere and crust: plume–arc interaction in the Abitibi–Wawa subduction accretion complex. *Precambr. Res.* **115**, 37–62 (2002).
7. Yuan, H. & Romanowicz, B. Lithospheric layering in the North American craton. *Nature* **466**, 1063–1068 (2010).
8. Martin, H., Smithies, R. H., Rapp, R., Moyen, J. F. & Champion, D. An overview of adakite, tonalite–trondhjemite–granodiorite (TTG), and sanukitoid: relationships and some implications for crustal evolution. *Lithos* **79**, 1–24 (2005).
9. Polat, A., Hofmann, A. W. & Rosing, M. T. Boninite-like volcanic rocks in the 3.7–3.8 Ga Isua greenstone belt, West Greenland: geochemical evidence for intra-oceanic subduction zone processes in the early Earth. *Chem. Geol.* **184**, 231–254 (2002).
10. Harrison, T. M. *et al.* Heterogeneous Hadean hafnium: evidence of continental crust at 4.4 to 4.5 Ga. *Science* **310**, 1947–1950 (2005).
11. van Thienen, P., Vlaar, N. J. & van den Berg, A. J. Assessment of the cooling capacity of plate tectonics and flood volcanism in the evolution of Earth, Mars and Venus. *Phys. Earth Planet. Inter.* **150**, 287–315 (2005).
12. Moresi, L., Dufour, F. & Muhlhaus, H.-B. A Lagrangian integration point finite element method for large deformation modeling of viscoelastic geomaterials. *J. Comput. Phys.* **184**, 476–497 (2003).
13. Nikolaeva, K., Gerya, T. V. & Marques, F. O. Subduction initiation at passive margins: numerical modeling. *J. Geophys. Res.* **115**, B03406 (2010).
14. Bailey, R. Gravity-driven continental overflow and Archaean tectonics. *Nature* **398**, 413–415 (1999).
15. Rey, P. F. & Coltice, N. Neoarchean lithospheric strengthening and the coupling of the Earth's geochemical reservoirs. *Geology* **36**, 635–638 (2008).
16. Bédard, J. H. A catalytic delamination-driven model for coupled genesis of Archaean crust and sub-continental lithospheric mantle. *Geochim. Cosmochim. Acta* **70**, 1188–1214 (2006).
17. Arndt, N. T., Coltice, N., Helmstaedt, H. & Michel, G. Origin of Archean subcontinental lithospheric mantle: some petrological constraints. *Lithos* **109**, 61–71 (2009).
18. Zhang, C. *et al.* Constraints from experimental melting of amphibolite on the depth of formation of garnet-rich restites, and implications for models of Early Archean crustal growth. *Precambr. Res.* **231**, 206–217 (2013).
19. Huppert, H. E. Propagation of two-dimensional and axisymmetric viscous gravity currents over a rigid horizontal surface. *J. Fluid Mech.* **121**, 43–58 (1982).
20. Moresi, L. & Solomatov, V. Mantle convection with a brittle lithosphere: thoughts on the global tectonic styles of the Earth and Venus. *Geophys. J. Int.* **133**, 669–682 (1998).
21. Demouchy, S., Tommasi, A., Ballaran, T. B. & Cordier, P. Low strength of Earth's uppermost mantle inferred from tri-axial deformation experiments on dry olivine crystals. *Phys. Earth Planet. Inter.* **220**, 37–49 (2013).
22. Zhong, S. & Watts, A. B. Lithospheric deformation induced by loading of the Hawaiian Islands and its implications for mantle rheology. *J. Geophys. Res.* **118**, 1–24 (2013).
23. van Hunen, J. & van den Berg, A. P. Plate tectonics on the early Earth: limitations imposed by strength and buoyancy of subducted lithosphere. *Lithos* **103**, 217–235 (2008).
24. Lenardic, A., Moresi, L.-N. & Mühlaus, H. Longevity and stability of cratonic lithosphere: insights from numerical simulations of coupled mantle convection and continental tectonics. *J. Geophys. Res.* **108**, 2303 (2003).
25. Sproule, R. A., Lesher, C. M., Ayer, J., Thurston, P. C. & Herzberg, C. T. Spatial and temporal variations in the geochemistry of komatiitic rocks in the Abitibi greenstone belt. *Precambr. Res.* **115**, 153–186 (2002).
26. Cazenave, A., Souriau, A. & Dominh, K. Global coupling of Earth surface topography with hotspots, geoid and mantle heterogeneities. *Nature* **340**, 54–57 (1989).
27. Ayer, J. *et al.* Evolution of the southern Abitibi greenstone belt based on U–Pb geochronology: autochthonous volcanic construction followed by plutonism, regional deformation and sedimentation. *Precambr. Res.* **115**, 63–95 (2002).
28. Bateman, R., Costa, S., Swe, T. & Lambert, D. Archaean mafic magmatism in the Kalgoorlie area of the Yilgarn Craton, Western Australia: a geochemical and Nd isotopic study of the petrogenetic and tectonic evolution of a greenstone belt. *Precambr. Res.* **108**, 75–112 (2001).
29. Kind, R., Yuan, X. & Kumar, P. Seismic receiver functions and the lithosphere–asthenosphere boundary. *Tectonophysics* **536–537**, 25–43 (2012).
30. Rolf, T. & Tackley, P. J. Focussing of stress by continents in 3D spherical mantle convection with self-consistent plate tectonics. *Geophys. Res. Lett.* **38**, L18301 (2011).

Author Contributions P.F.R. conceived the study. P.F.R. and N.C. performed numerical experiments. P.F.R., N.C. and N.F. interpreted the results. P.F.R., N.C. and N.F. wrote the manuscript.

Author Information Reprints and permissions information is available at www.nature.com/reprints. The authors declare no competing financial interests. Readers are welcome to comment on the online version of the paper. Correspondence and requests for materials should be addressed to P.F.R. (patrice.rey@sydney.edu.au).

METHODS

We solve the problem of conservation of mass, momentum and energy for incompressible mantle flow and lithosphere deformation in the top 700 km of the Earth by using the particle-in-cell finite-element code Ellipsis[12,31] (freely available at http://www.geodynamics.org/cig/software/ellipsis3d/; the specific version of Ellipsis and input scripts used for this work are available from the first author on request.). Our reference Cartesian two-dimensional numerical model is 6,300 km long. The Stokes equation that balances buoyancy forces, viscous stresses and pressure gradients is solved on an Eulerian computational grid made of 32×288 cells with uniform spacing. We have verified the validity of our results by testing a higher-resolution grid of 64×576 cells. Each cell is populated with 100 Lagrangian particles (total $>920,000$ particles) tracking the material properties and therefore material interfaces during mantle flow and lithospheric deformation. A free-slip condition is applied to the vertical and horizontal boundaries of the modelling domain. The temperature at the upper horizontal boundary is maintained at 293 K, and the base is maintained at 1,873 K. More than 200 calculations were conducted, varying the lateral extent of the model domain (4,200–16,800 km), the half-width (400–1,400 km) and thickness (175 or 225 km) of the continents, the limiting yield stress of mantle rocks (100–500 MPa), the density of the top 75 km of the oceanic lid mantle (3,395 down to 3,360 kg m^{-3}), and various modes of melt extraction.

Each material is characterized by a range of thermal and mechanical properties (Extended Data Table 1), including density, coefficient of thermal expansion, heat capacity (1,000 J kg^{-1} K^{-1}), heat diffusivity (9×10^{-7} m^2 s^{-1}), radiogenic heat production, cohesion, coefficient of friction, limiting pressure-independent yield stress, dislocation creep parameters (A, n, E; Extended Data Table 1) and limiting lower and upper viscosities, respectively 10^{18} and 5×10^{23} Pa s.

Our strategy consists of setting up a model in which the mantle convects under a stagnant lid, the top 15 km of which are made of weak basaltic crust simulating hydrothermally altered basalts (Extended Data Fig. 2). After reaching steady-state equilibrium, the temperature field is laterally averaged (Extended Data Fig. 2) and linearized (that is, temperature at the surface is 293 K and the temperature at 150 km depth and below is 1,820 K). This ensures that no convective stress acts on the lid in the initial condition. Finally, we replace a segment of the oceanic lid by a continent made of depleted mantle underneath a continental crust. We take advantage of the symmetry of the model, and insert the continent along the left side of the model.

We model the mantle as a visco-plastic material with viscosity dependent on temperature, stress, strain rate, melt fraction and depletion. The rheology of the mantle is based on dry olivine[32] (Extended Data Table 1). Its plastic rheology is approximated by a Coulomb failure criterion[33] with cohesion 40 MPa, a coefficient of friction (μ_{ref}) 0.268 and a weakening factor dependent on the accumulated plastic strain (ε_p). The coefficient of friction (μ) evolves as a function of the total plastic strain as

$$\mu = \mu_{ref} \times [1 - (1 - 0.0373) \times (\varepsilon_p/0.15)^{0.25}]$$

for $\varepsilon_p < 0.15$, and

$$\mu = \mu_{ref} \times 0.0373$$

for $\varepsilon_p > 0.15$.

This weakening leads to fault-like strain localization with nominal viscosity ~25-fold weaker than that of the surrounding rocks when plastic strain reaches 15%. This weakening, which is a key factor for the operation of plate tectonics on present Earth[20], simulates the formation of phyllosilicates (serpentine, talc and micas) during the strain-induced hydration of mantle rocks and basalts. For semi-brittle deformation independent of pressure, we impose an upper limiting yield stress[34,35] in the range 100–500 MPa.

The top 15 km of the model consists of a thick layer of basalts, which simulates both the oceanic crust and the greenstone cover on the Archaean continent. Because these basalts were largely emplaced below sea level[36], they are strongly hydrothermally altered. For simplicity we assume that this layer has a nominal viscosity 1,000-fold weaker than that of the underlying mantle, a weak cohesion of 1 MPa, a reference coefficient of friction of 0.134 and the same weakening properties as the rest of the lid. This weak layer of basalt helps the decoupling between the subducting slab and the upper plate, permitting one-sided subduction. It also mitigates the absence of a free surface, by allowing the upper plate to bend downwards more realistically to form a deeper trench. The reference density of this material (3,000 kg m^{-3}) is sensitive to pressure, and increases to 3,540 kg m^{-3} on burial, to simulate eclogitization[37]. When subduction is initiated, this weak material lubricates the Benioff plane, which, with eclogitization, facilitates subduction by decoupling the slab from the continental

margin. This simulates the impact of slab dehydration, which in nature lubricates the Benioff plane.

Modelling continent differentiation is beyond the scope of this paper, and we simply replace a 400–1,200-km-long segment of the oceanic lid by a continent, which includes a crust 40 km thick (density 2,850 kg m^{-3}), covered by a flood basalt 15 km thick (density 3,000 kg m^{-3}). This crust stands above 170 km of depleted mantle (density 3,310 kg m^{-3}) with a nominal viscosity 100-fold stronger than the adjacent lid to account for dehydration[38]. We assume the same limiting yield stress as that of other mantle rocks that we vary in the range 100–500 MPa. The continental crust is assumed to be 100-fold more viscous than a weak mafic granulite[39] (Extended Data Table 1). A limiting yield stress of 250 MPa is imposed in the crust to simulate a semi-brittle regime. This strong continent represents a significant buoyant anomaly, imparting a horizontal gravitational force on its surroundings.

We use the hydrous mantle solidus and liquidus of ref. 40 to model partial melting in the sub-continental fertile mantle. For the depleted root of the continent we increase the hydrous-mantle solidus by 200 K, a reasonable assumption for the harzburgite solidus[41]. Melt fraction is calculated at each time step by using equation (21) of ref. 42, whereas the MgO content of accumulated melt in Fig. 2 is calculated by using ref. 43. Because decompression and exhumation of the mantle occur very slowly (~1–4 mm per year), at the pace imposed by the spreading of the continent, one can expect the melt to segregate and to pond at the top of the partially molten column, before it escapes to the surface through dikes. We therefore assume that melt in the partially molten column is extracted when the melt fraction reaches 1%. In this case, latent heat escapes with the melt, and the ascending depleted residue follows the solidus closely. We assume the fusion entropy to be 400 J kg^{-1} K^{-1}. We have also tested the isentropic case in which the melt stays in the source. In this case, lithospheric boudinage controls continental spreading, rather than the homogeneous thinning.

The small amount of melt trapped in the rocks ($<1\%$) has only a modest impact on the buoyancy of the partially molten region. However, the density of the residue decreases as it becomes more depleted. We assume a maximum density decrease of 1.5% on full depletion. Because even a small fraction of melt lubricates grain boundaries, it affects the viscosity of the partially molten column. We therefore impose a linear decrease in viscosity to a maximum of one order of magnitude when the melt fraction reaches 1%. However, partial melting drains water out of the solid matrix and reduces the number of phases. Although the impact of dehydration on the viscosity may not be as significant as previously thought[44], both processes should contribute to an increase in the viscosity of the depleted residue once its temperature drops below the solidus. In our experiment we impose an increase in viscosity proportional to depletion, assuming an increase in viscosity of two orders of magnitude for 100% depletion.

31. O'Neill, C., Moresi, L., Müller, R. D., Albert, R. & Dufour, F. Ellipsis 3D: a particle-in-cell finite-element hybrid code for modelling mantle convection and lithospheric deformation. *Comput. Geosci.* **32,** 1769–1779 (2006).
32. Brace, W. F. & Kohlstedt, D. L. Limits on lithospheric stress imposed by laboratory experiments. *J. Geophys. Res.* **85,** 6248–6252 (1980).
33. Byerlee, J. D. Brittle–ductile transition in rocks. *J. Geophys. Res.* **73,** 4741–4750 (1968).
34. Ord, A. & Hobbs, B. E. The strength of the continental crust, detachment zones and the development of plastic instabilities. *Tectonophysics* **158,** 269–289 (1989).
35. Escartin, J. & Hirth, G. Nondilatant brittle deformation of serpentinites: implications for Mohr–Coulomb theory and the strength of faults. *J. Geophys. Res.* **102,** 2897–2913 (1997).
36. Flament, N., Coltice, N. & Rey, P. F. A case for late-Archaean continental emergence from thermal evolution models and hypsometry. *Earth Planet. Sci. Lett.* **275,** 326–336 (2008).
37. Aoki, I. & Takahashi, E. Density of MORB eclogite in the upper mantle. *Phys. Earth Planet. Inter.* **143–144,** 129–143 (2004).
38. Hirth, G. & Kohlstedt, D. in *Inside the Subduction Factory* (ed. Eiler, J.) 83–105 (Geophysical Monograph no. 138, American Geophysical Union, 2003).
39. Wang, Y. F., Zhang, J. F., Jin, Z. M. & Green, H. W. Mafic granulite rheology: implications for a weak continental lower crust. *Earth Planet. Sci. Lett.* **353–354,** 99–107 (2012).
40. Katz, R. F., Spiegelman, M. & Langmuir, C. H. A new parameterization of hydrous mantle melting. *Geochem. Geophys. Geosyst.* **4,** 1073 (2003).
41. Maaløe, S. The solidus of harzburgite to 3 GPa pressure: the compositions of primary abyssal tholeiite. *Mineral. Petrol.* **81,** 1–17 (2004).
42. McKenzie, D. & Bickle, M. J. The volume and composition of melt generated by extension on the lithosphere. *J. Petrol.* **29,** 625–629 (1988).
43. Herzberg, C. & Gazel, E. Petrological evidence for secular cooling in mantle plumes. *Nature* **458,** 619–623 (2009).
44. Fei, H., Wiedenbeck, M., Yamazaki, D. & Katsura, T. Small effect of water on upper-mantle rheology based on silicon self-diffusion coefficients. *Nature* **498,** 213–216 (2013).
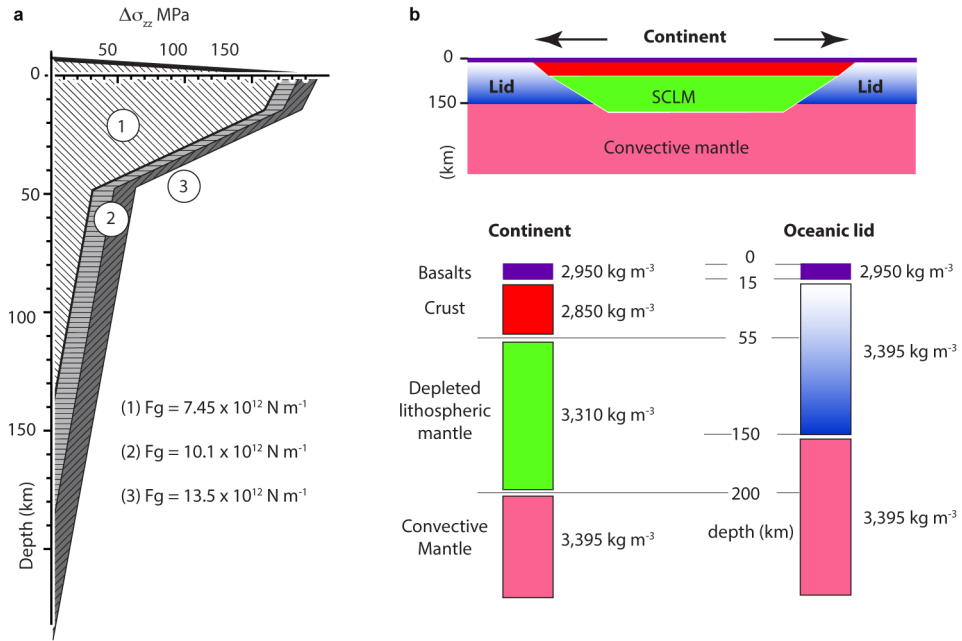
Extended Data Figure 1 | Gravitational force between continent and oceanic lid. a, Depth profile of the difference in lithostatic pressure σ_{zz} between an oceanic lid 150 km thick and a continent (1) 150 km thick, (2) 200 km thick and (3) 250 km thick. The vertical integration of the lithostatic pressure difference ($\Delta\sigma_{zz}$) is the resulting gravitational force F_g acting between the Archaean continent and the adjacent lithospheric lid. In all cases, this force is $>7 \times 10^{13}$ N m^{-1}, comparable to or larger than the present-day tectonic forces driving orogenesis[1]. **b**, Reference density structure of the continent and oceanic lithosphere (densities of depleted and fertile mantle are from ref. 5). All densities vary with temperature with a coefficient of thermal expansion $\alpha = 3 \times 10^{-5}$ K^{-1}. We assume a linear geotherm in the oceanic plate ($T_{(z=0)} = 293$ K, $T_{(z=150\,km)} = 1,820$ K) above a convective mantle with an average temperature of 1,820 K.
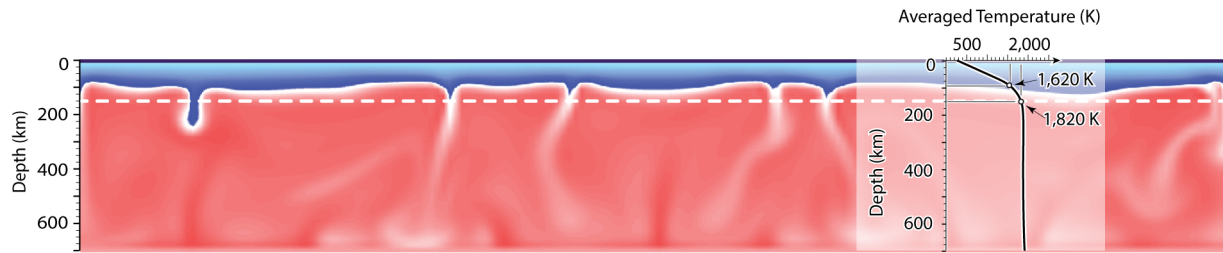
Extended Data Figure 2 | Stagnant-lid convection model before lateral averaging and introduction of a continent. The temperature field in our experiments derives from the lateral averaging of an experiment in which the mantle is allowed to convect under constant upper-boundary temperatures (293 K) and internal production of radiogenic heat ($1.36 \times 10^{-8}\,W\,m^{-3}$). The thermal expansion is $3 \times 10^{-5}\,K^{-1}$, the thermal diffusivity is $0.9 \times 10^{-6}\,m^2\,s^{-1}$, the heat capacity is $1{,}000\,J\,kg^{-1}\,K^{-1}$, and the Rayleigh number of the convecting mantle is between 10^6 and 10^7. The snapshot shows the temperature field after ~1 Gyr of evolution. In this experiment, a lid develops and remains stagnant. Conductive cooling and the formation of cold drips from the lower, unstable part of the stagnant lid balance each other out to maintain the thickness of the stagnant lid. In the lid, the conductive geotherm is such that a temperature of 1,620 K is reached at ~100 km depth, and 1,820 K (the average temperature in the convecting mantle) is reached at ~150 km depth.
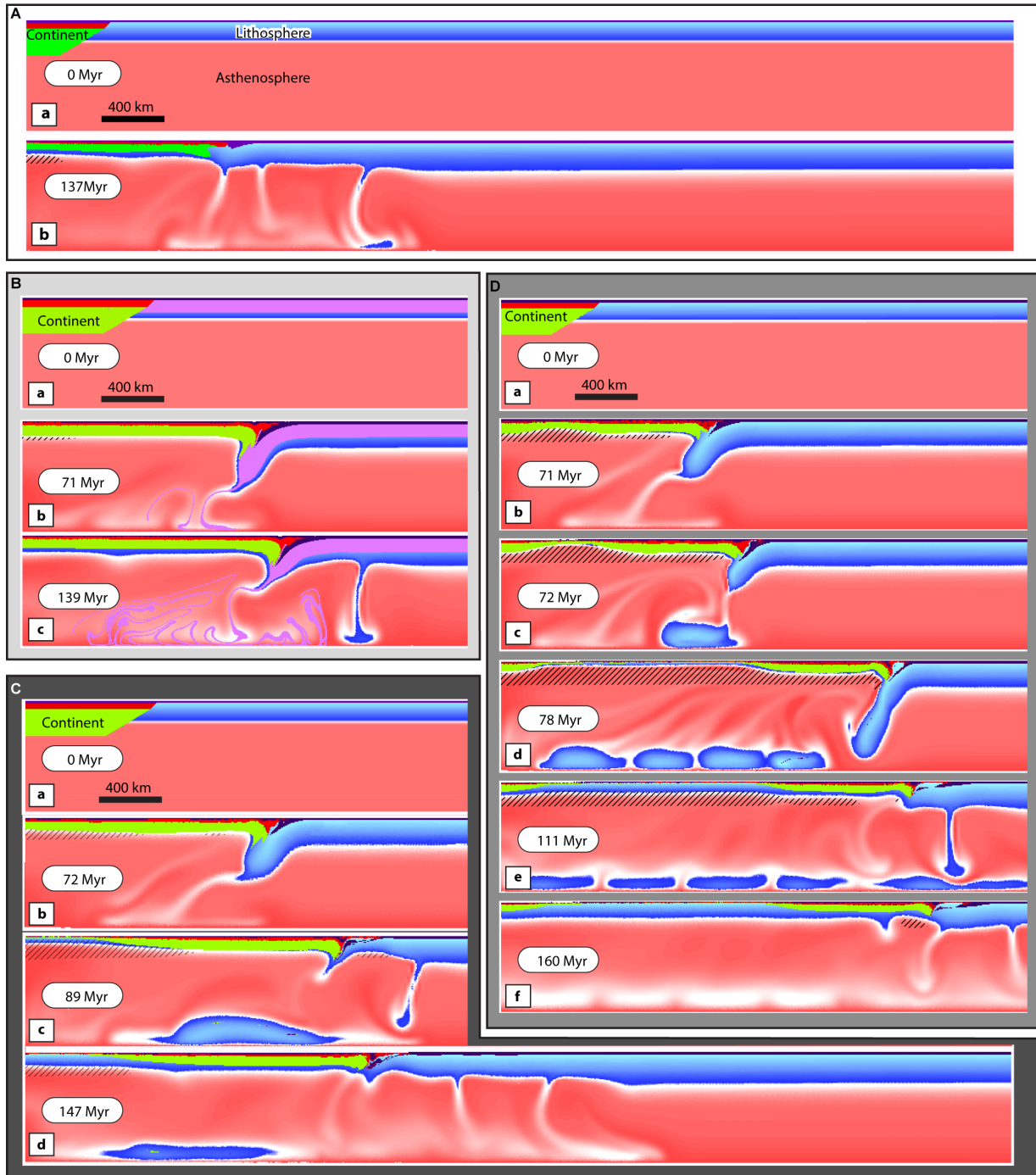
Extended Data Figure 3 | Numerical solutions for various models showing contrasting tectonic evolutions. A, In this experiment, all parameters are as in Fig. 1 except the continent half-width, which is 500 km. In the case of stable continental collapse, cold drips form faster than subduction can initiate, which stabilizes the oceanic lid. **a**, Initial state. **b**, During and after spreading and thinning of the continent, a layer of mostly fertile mantle is accreted at the base of the continent through cooling. **B**, This experiment is in all aspects similar to that presented in Fig. 1 except for the oceanic lid, which includes 75 km of buoyant lithopheric mantle (in purple) with a reference density of 3,365 kg m^{-3} (that is, 35 kg m^{-3} less dense than non-depleted mantle rocks). **a**, **b**, Homogeneous continental spreading with decompression melting, and the initiation of a slab that stalls underneath a long-lived orogenic wedge. The same experiment with a buoyant mantle lid with a reference density of 3,370 kg m^{-3} leads to subduction. **c**, The very base of the oceanic slab is dragged into the asthenosphere. **C**, In this experiment the limiting yield stress of the strongly depleted continental mantle (in green) is increased to 500 MPa to take

into account the possible plastic strengthening of the depleted—and therefore dry—mantle (all other mantle rocks have a limiting yield stress of 300 MPa). Comparison with Fig. 1—which shows the same experiment but with all mantle rocks having a limiting yield stress of 300 MPa—illustrates that a stronger continent deforms in a more heterogeneous manner. After an episode of spreading, thinning and subduction initiation (**b**), strain localization and rifting divide the continent in two as the slab detaches (**c**) before stabilization and cooling (**d**). **D**, In this experiment, the continent has a half width of 600 km (**a**), and all mantle rocks have a limiting yield stress of 200 MPa. **b**–**d**, Continental rifting, recurrent slab detachment and trench-retreat occur, and two continental blocks move away from each other with little internal deformation. **e**, **f**, Rifting and subduction stop, while cooling re-establishes a stagnant lid. In all cases, a protracted phase of decompression melting lasting several tens of millions of years is coeval with spreading and rifting.
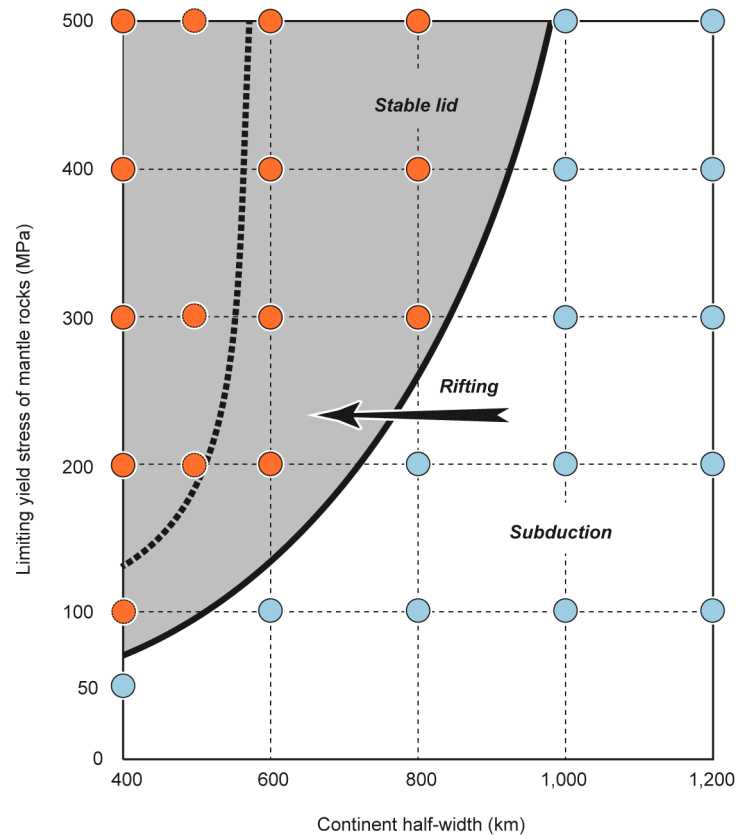
Extended Data Figure 4 | Tectonic phase diagram: subduction versus stable-lid regime as a function of yield stress and continent width. Two series of calculations were performed (with continental thicknesses of 175 and 225 km), systematically varying the half-width of the continent (from 400 to 1,200 km) and the limiting yield stress of all mantle rocks (from 100 to 500 MPa). Depending on the competition between the gravitational driving power of the buoyant continent and the combined viscous resistance of the continent and oceanic lid, the continental collapse may or may not lead to the subduction of the oceanic lid under the continental margin. Coloured dots and the continuous black thick line represent the outcomes of numerical experiments for the 175-km-thick continent. The thick dashed line separates the stable-lid domain from the subduction domain in the case of the 225-km-thick continent. The arrow illustrates that continental rifting, because it reduces the half-width of continents, stabilizes Archaean oceanic lids.

Extended Data Table 1 | Thermal and mechanical parameters

	Reference density (kg m^{-3})	Thermal expansion (K^{-1})	Radiogenic Heat (W kg^{-1})	Cohesion (MPa)	Coefficient of friction	Limiting yield stress (MPa)	A (MPa^{-n} s^{-1})	E (kJ mol^{-1})	n
Continental crust	2,850	0	2.52×10^{-10}	40	0.268	250	2×10^{-2}	244	3.2
Basalts	3,000	0	2.52×10^{-10}	1	0.134	50	7×10^{7}	520	3.0
SCLM	3,310	3×10^{-5}	4×10^{-12}	40	0.268	100-500	7×10^{2}	520	3.0
Mantle	3,395	3×10^{-5}	4×10^{-12}	40	0.268	100-500	7×10^{4}	520	3.0